

First-principles exploration of superconductivity in MXenes

Supplementary Information

J. Bekaert,¹ C. Sevik,² and M. V. Milošević¹

¹Department of Physics & NANOLab Center of Excellence, University of Antwerp, Groenenborgerlaan 171, B-2020 Antwerp, Belgium

²Department of Mechanical Engineering, Faculty of Engineering, Eskisehir Technical University, 26555 Eskisehir, Turkey

FERMI SURFACES

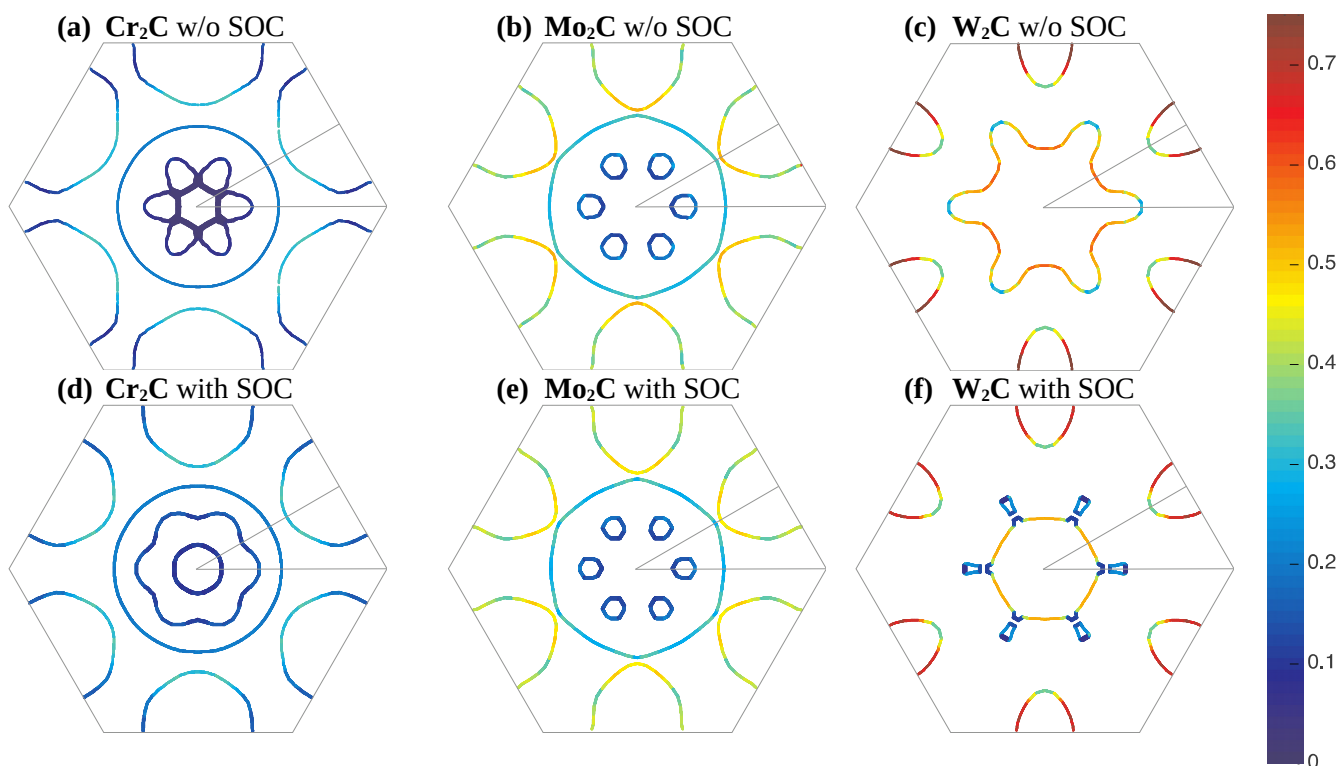


Figure 1: Calculated Fermi surfaces. Line color shows the calculated Fermi velocity in 10^6 ms^{-1} .

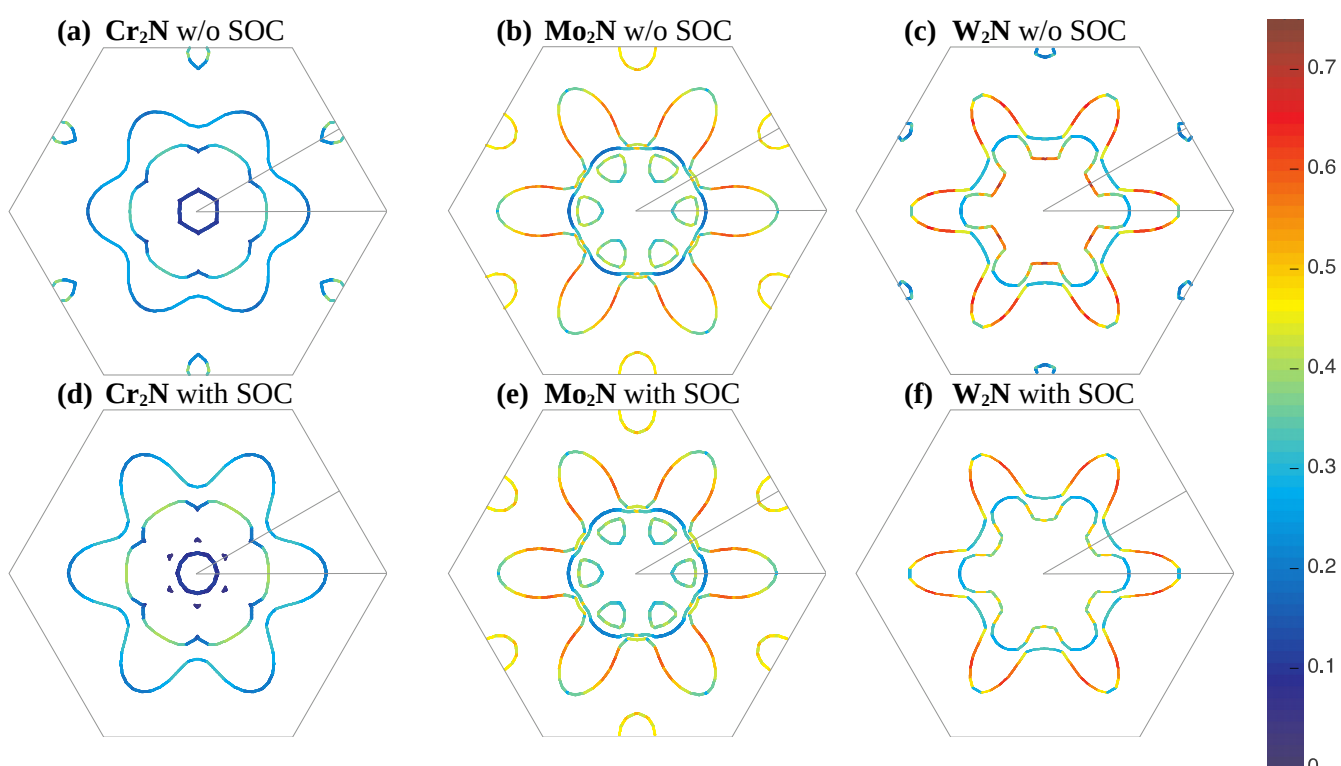


Figure 2: Calculated Fermi surfaces. Line color shows the calculated Fermi velocity in 10^6 ms^{-1} .

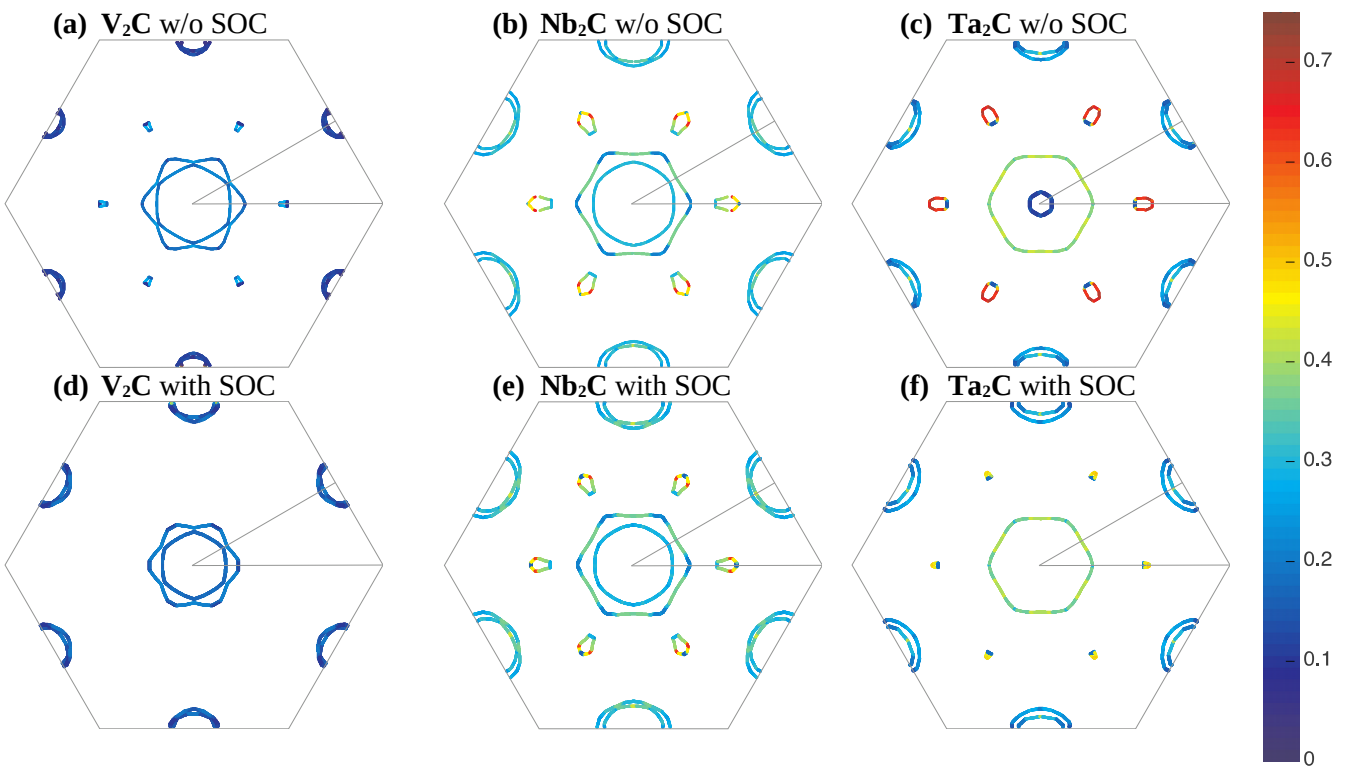


Figure 3: Calculated Fermi surfaces. Line color shows the calculated Fermi velocity in 10^6 ms^{-1} .

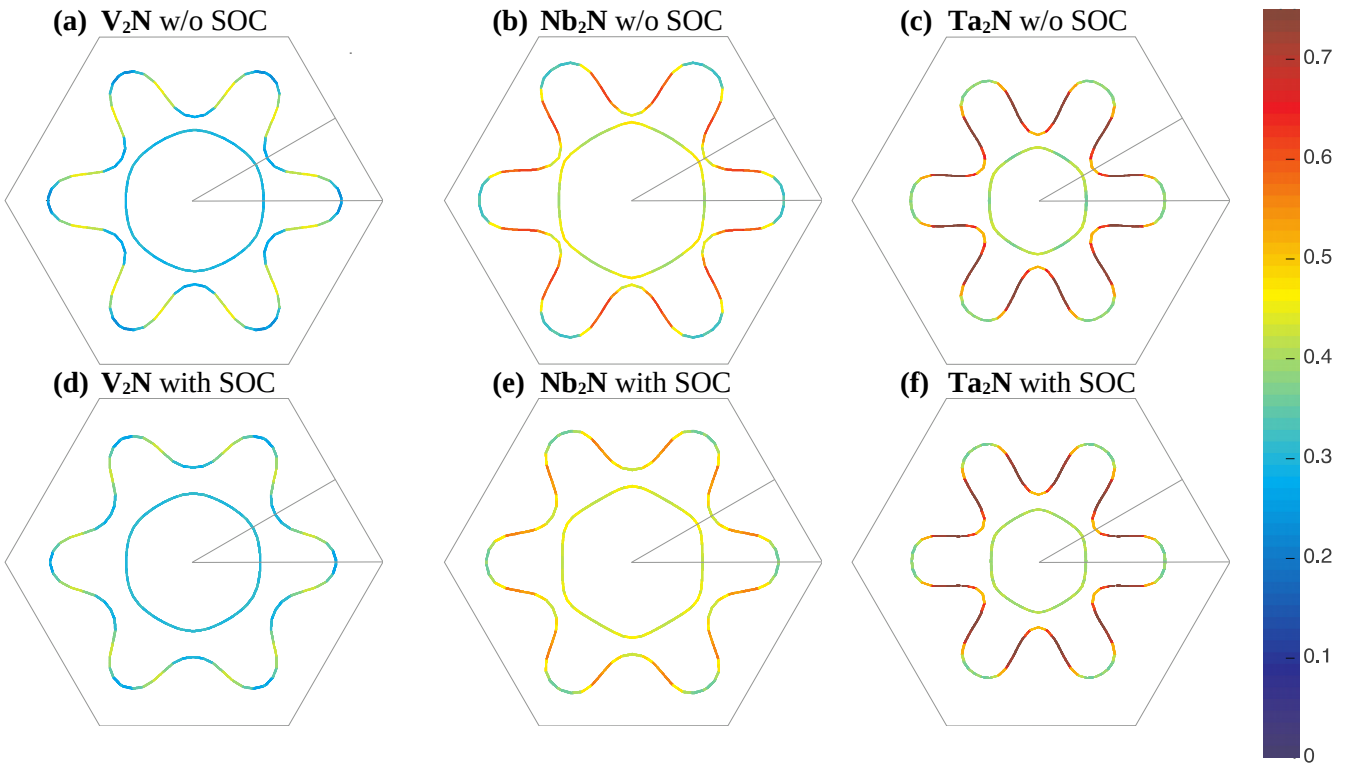


Figure 4: Calculated Fermi surfaces. Line color shows the calculated Fermi velocity in 10^6 ms^{-1} .

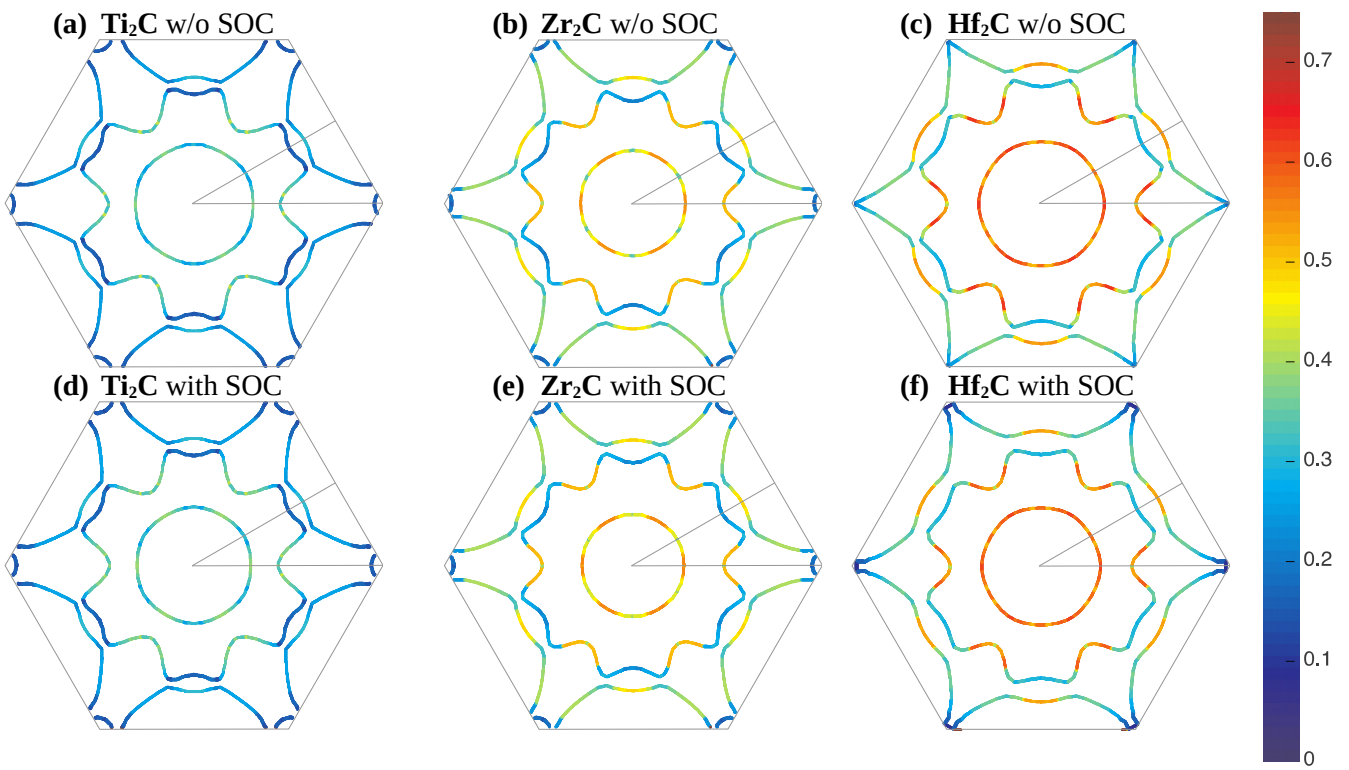


Figure 5: Calculated Fermi surfaces. Line color shows the calculated Fermi velocity in 10^6 ms^{-1} .

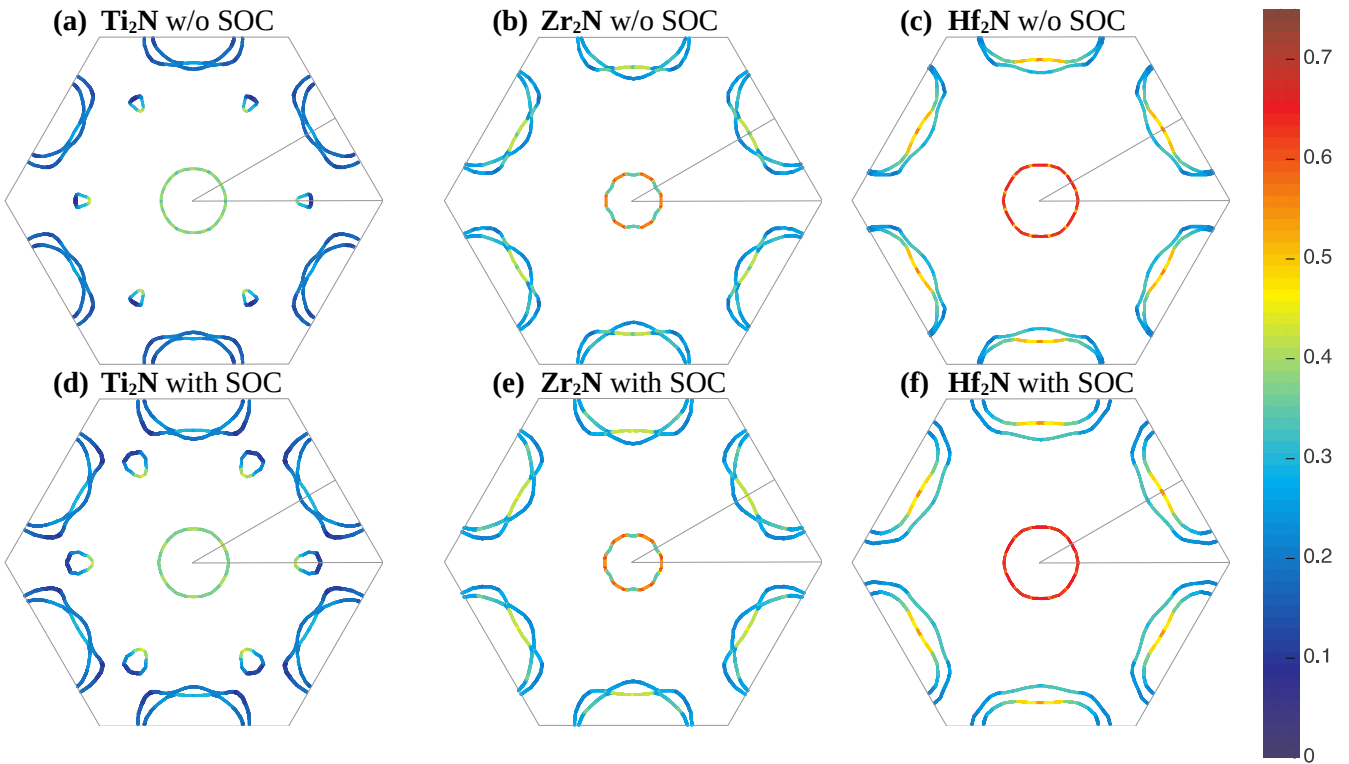


Figure 6: Calculated Fermi surfaces. Line color shows the calculated Fermi velocity in 10^6 ms^{-1} .

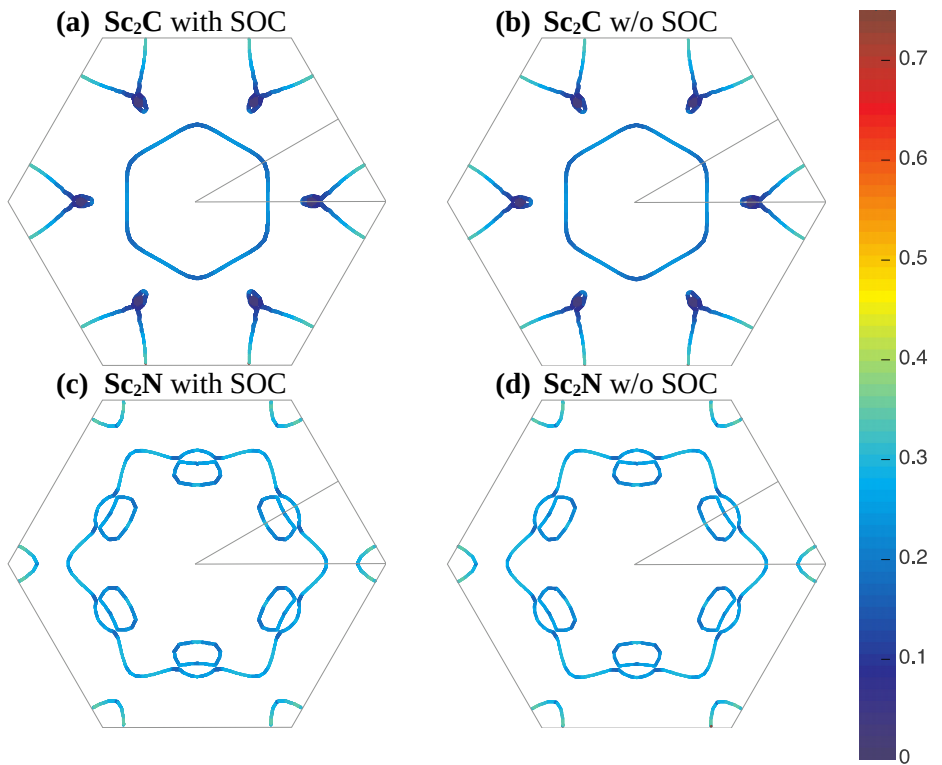


Figure 7: Calculated Fermi surfaces. Line color shows the calculated Fermi velocity in 10^6 ms^{-1} .

ELECTRON-PHONON COUPLING – CARBIDES

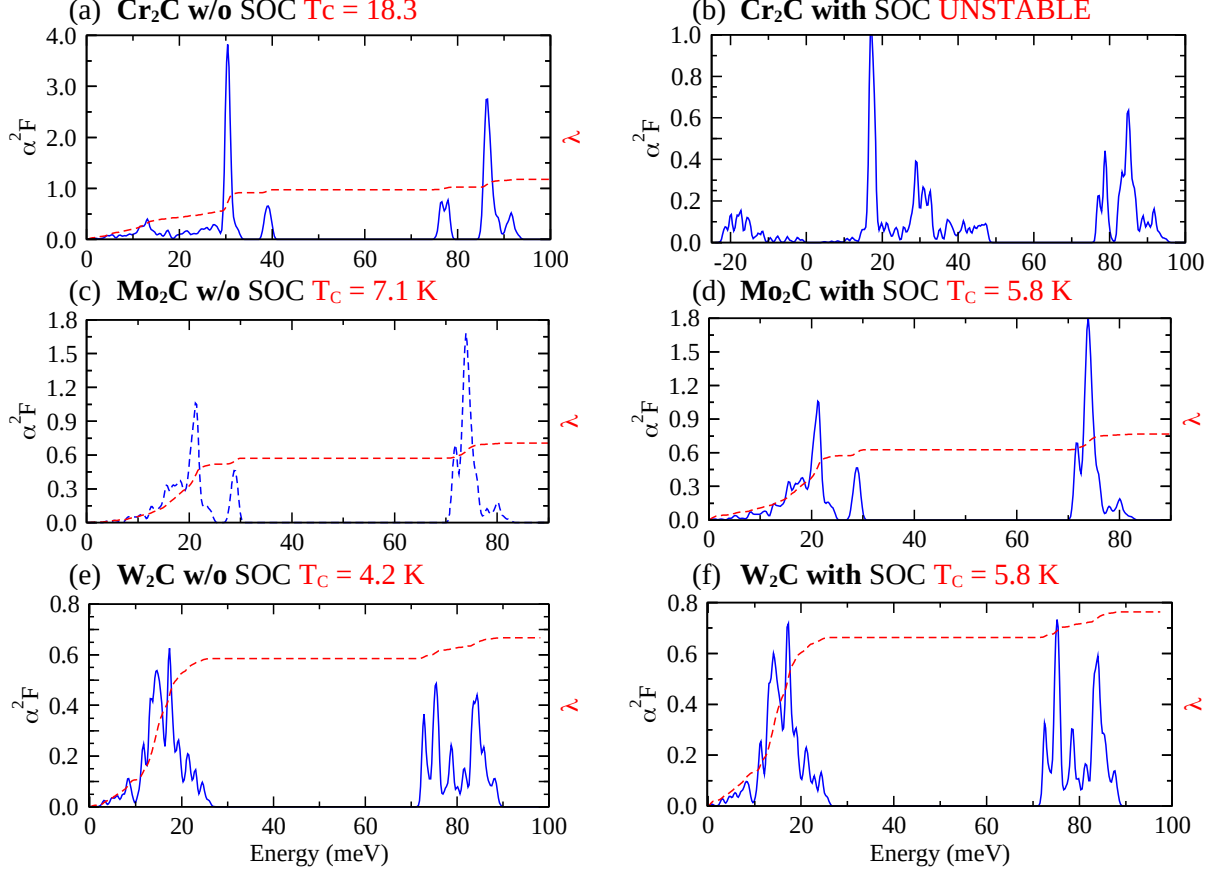


Figure 8: The isotropic Eliashberg function $\alpha^2 F(\omega)$ and resulting electron-phonon coupling λ .

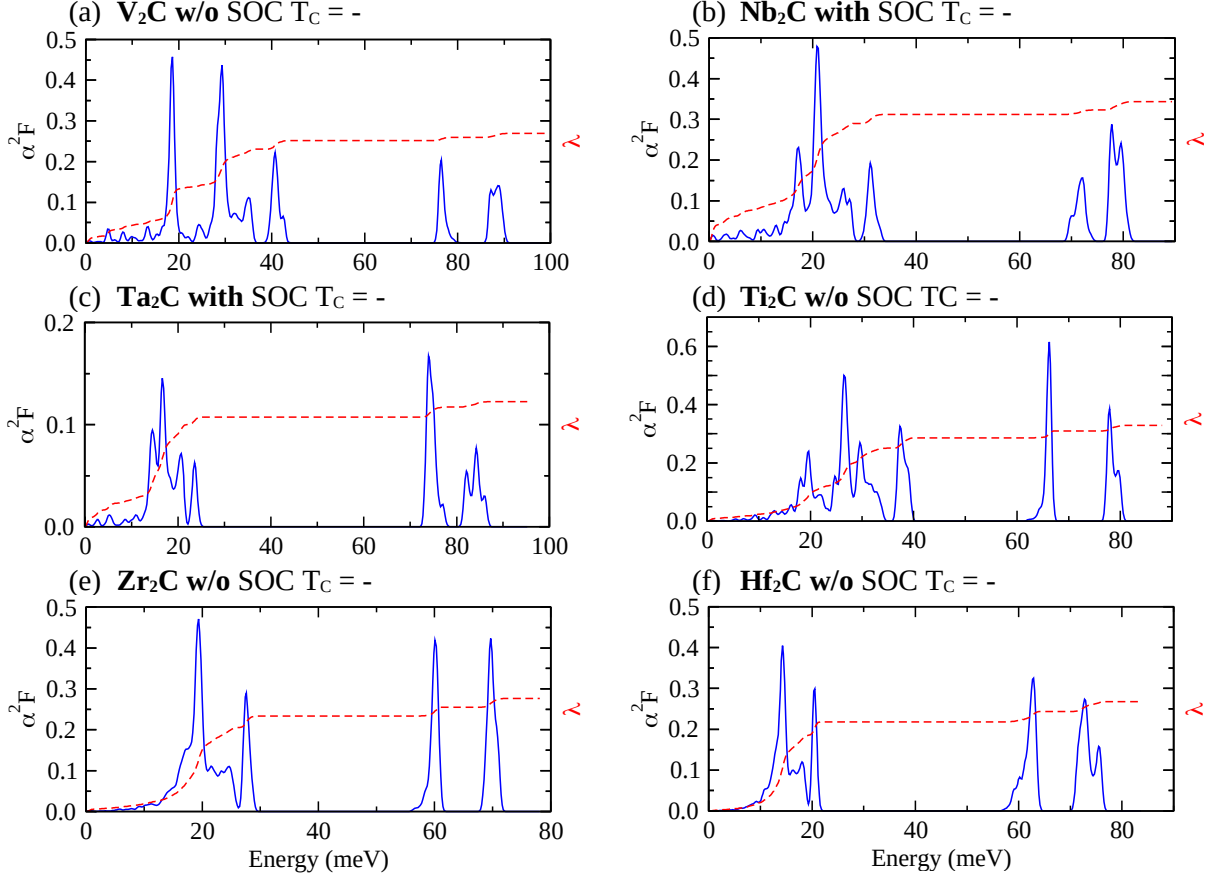


Figure 9: The isotropic Eliashberg function $\alpha^2 F(\omega)$ and resulting electron-phonon coupling λ .

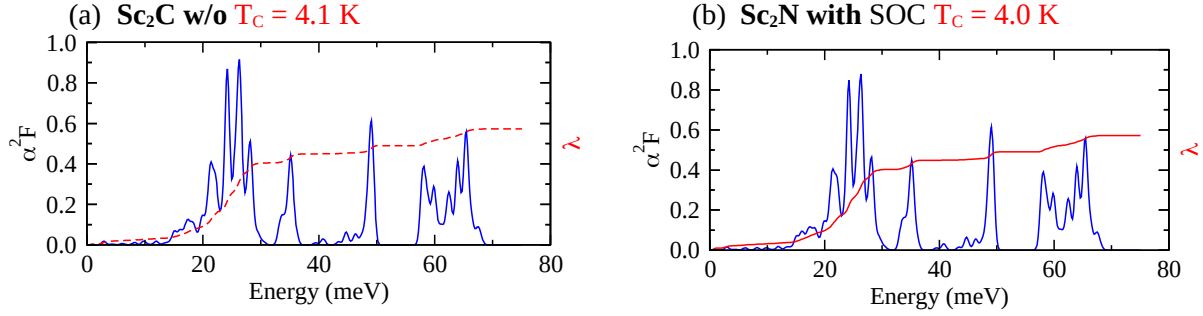


Figure 10: The isotropic Eliashberg function $\alpha^2 F(\omega)$ and resulting electron-phonon coupling λ .

ELECTRON-PHONON COUPLING – NITRIDES

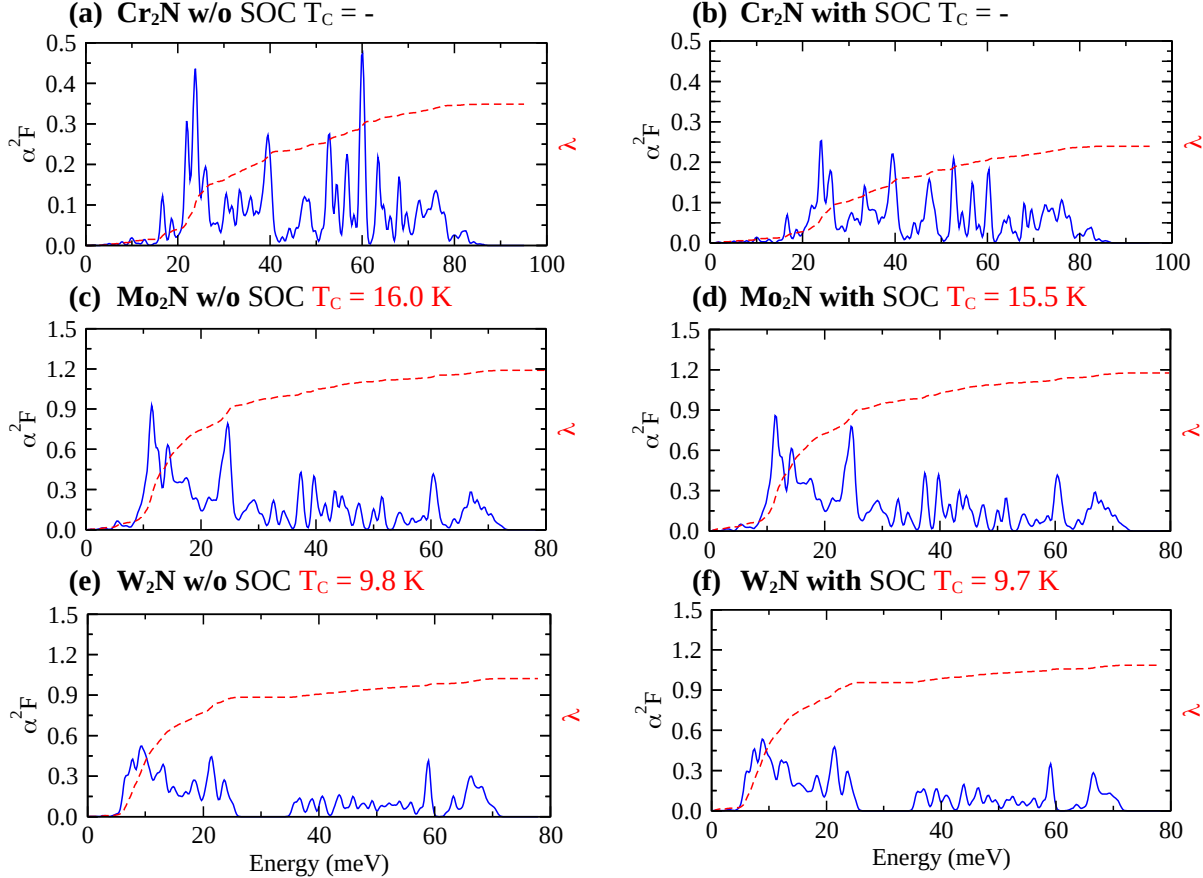


Figure 11: The isotropic Eliashberg function $\alpha^2 F(\omega)$ and resulting electron-phonon coupling λ .

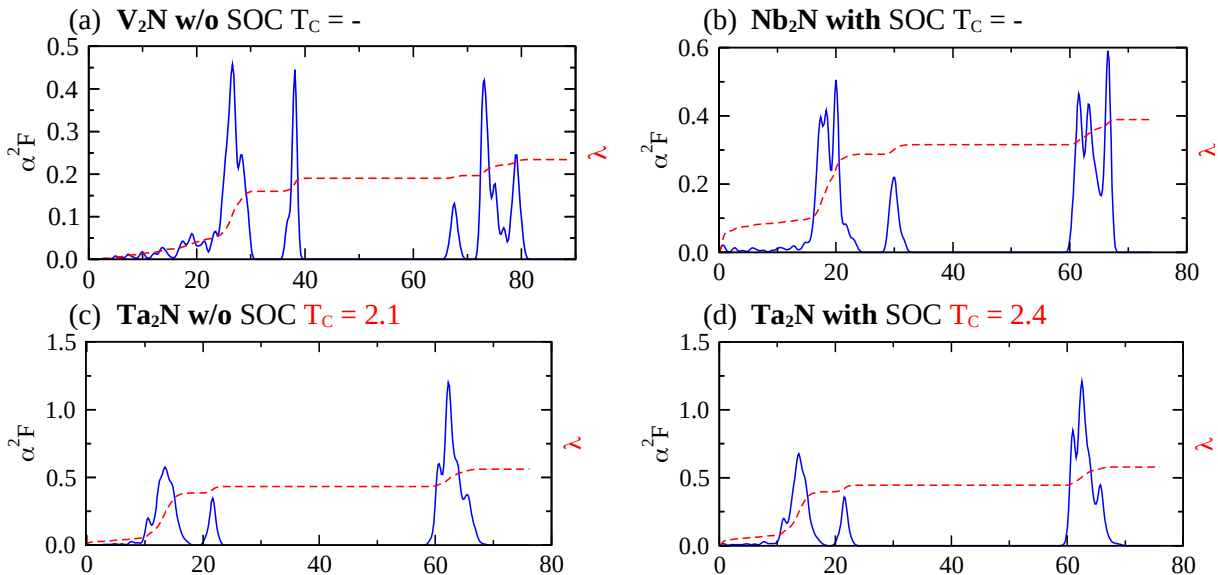


Figure 12: The isotropic Eliashberg function $\alpha^2 F(\omega)$ and resulting electron-phonon coupling λ .

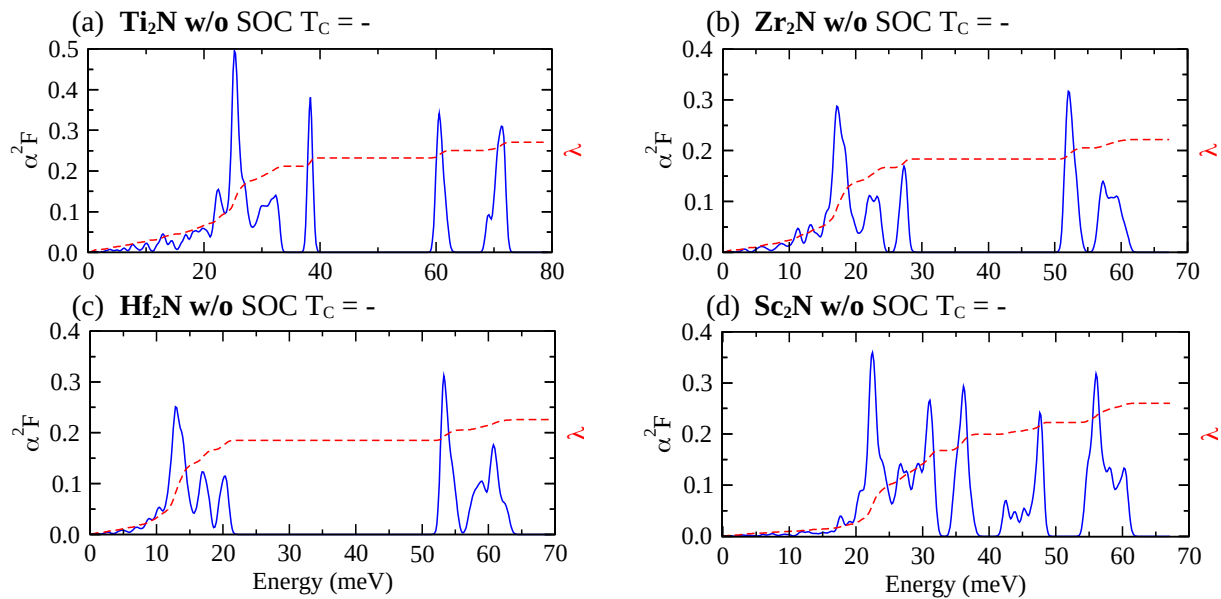


Figure 13: The isotropic Eliashberg function $\alpha^2 F(\omega)$ and resulting electron-phonon coupling λ .

BAND STRUCTURES – CARBIDES

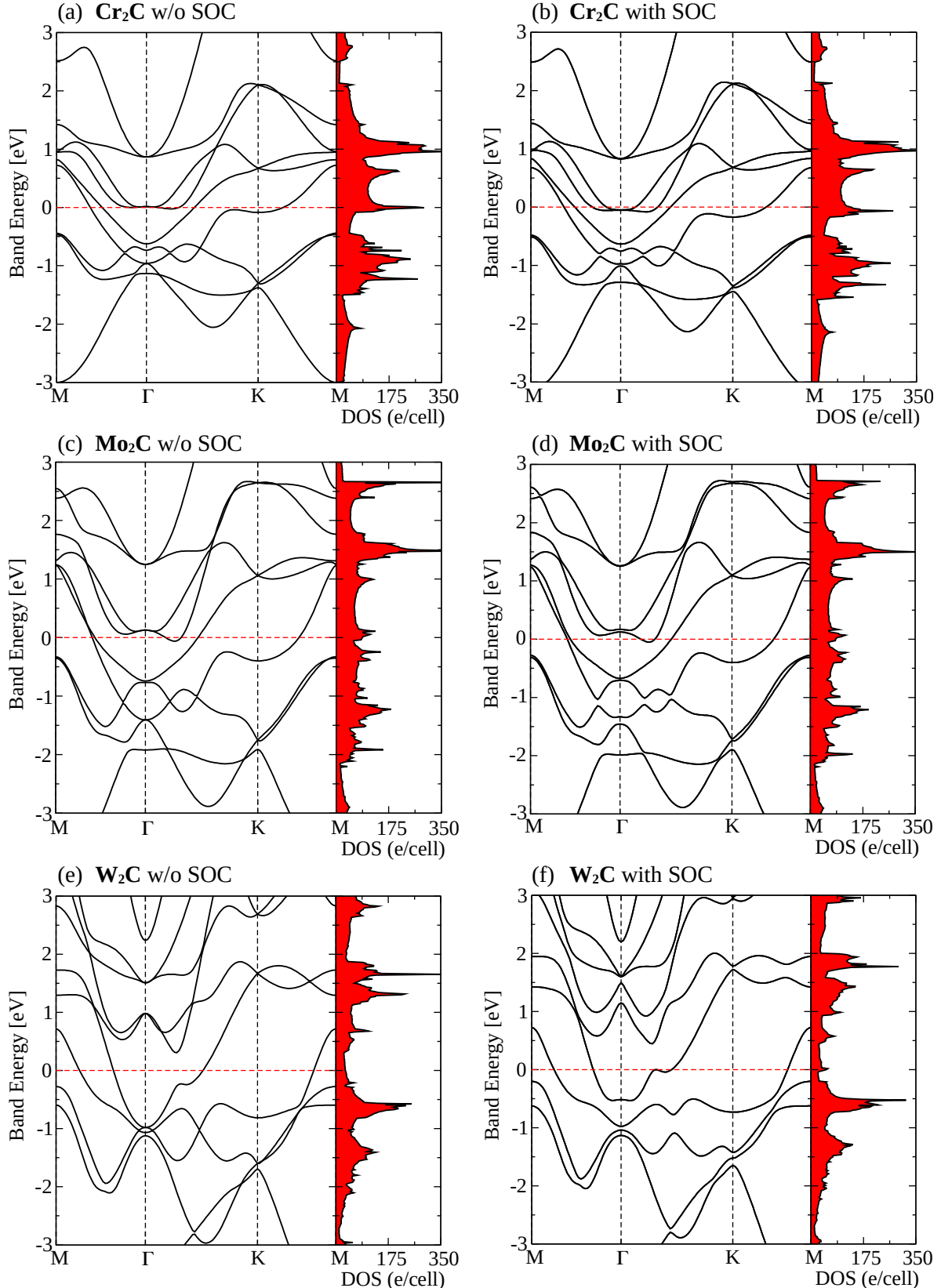


Figure 14: The band structure of M_2C ($M = Cr, Mo, W$) with and without spin-orbit coupling, along the high-symmetry directions of the hexagonal Brillouin zone. DOS in electrons/Hartree/cell.

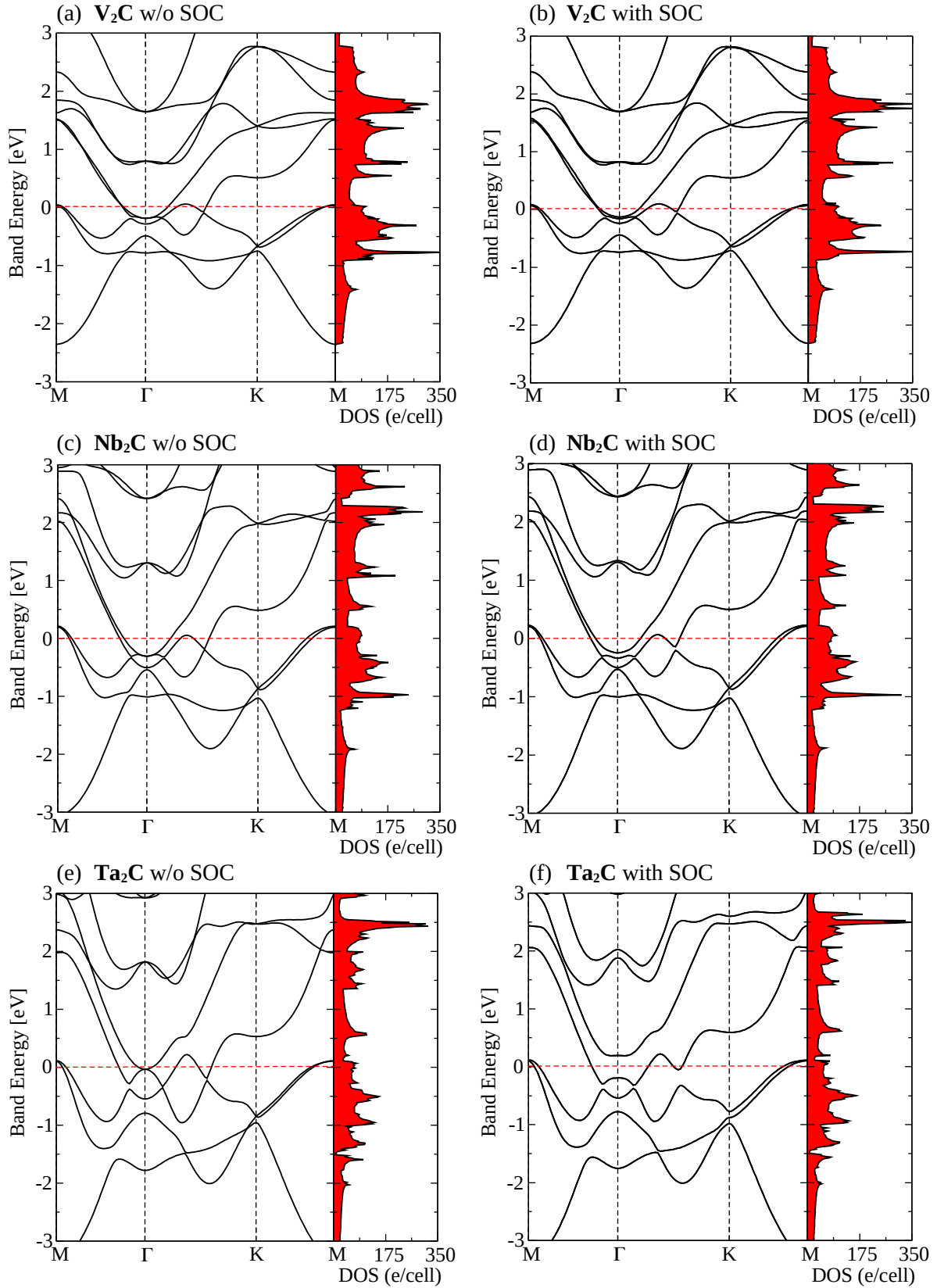


Figure 15: The band structure of M_2C ($M = V, Nb, Ta$) with and without spin-orbit coupling, along the high-symmetry directions of the hexagonal Brillouin zone. DOS in electrons/Hartree/cell.

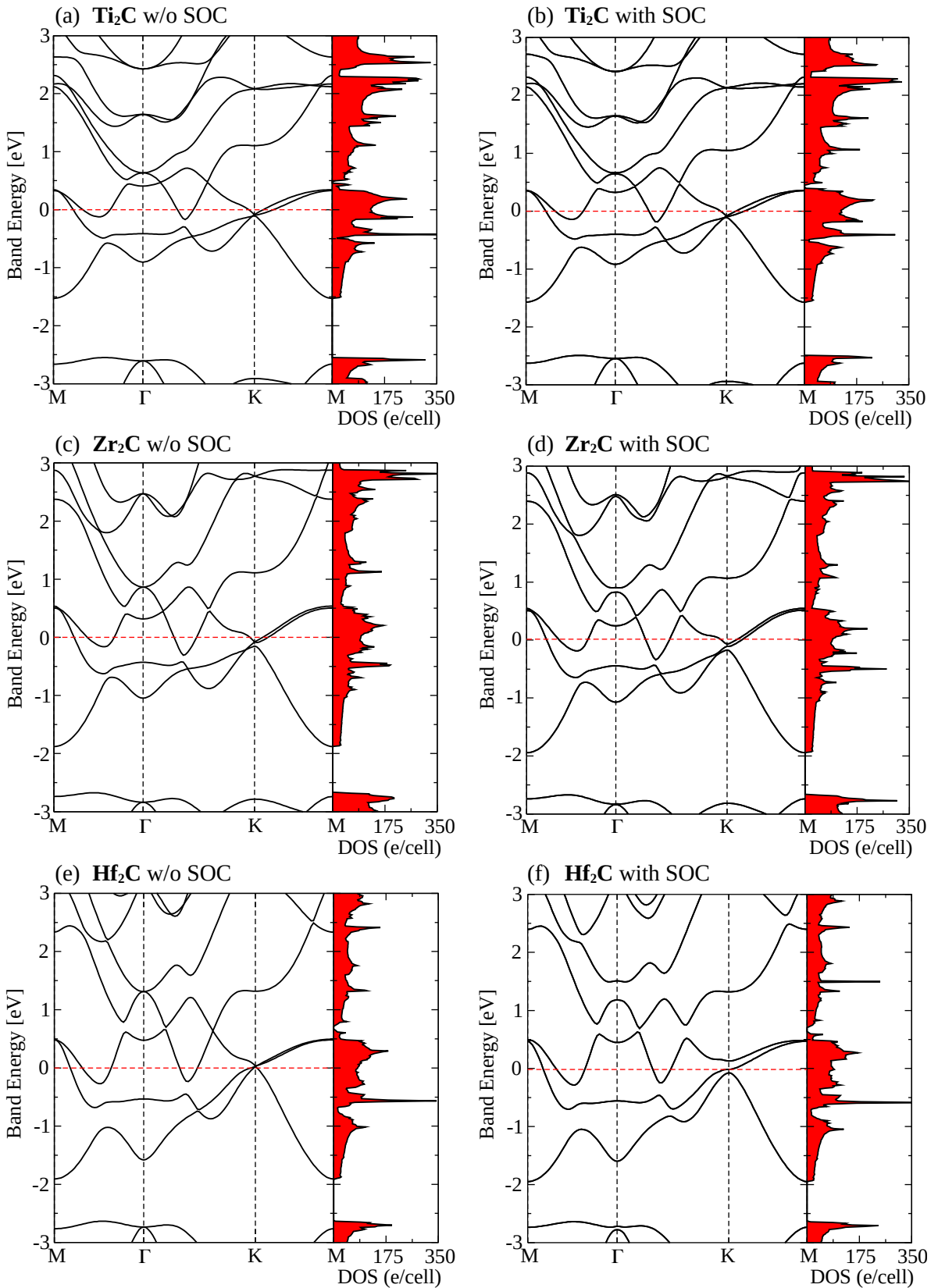


Figure 16: The band structure of M_2C ($\text{M} = \text{Ti}, \text{Zr}, \text{Hf}$) with and without spin-orbit coupling, along the high-symmetry directions of the hexagonal Brillouin zone. DOS in electrons/Hartree/cell.

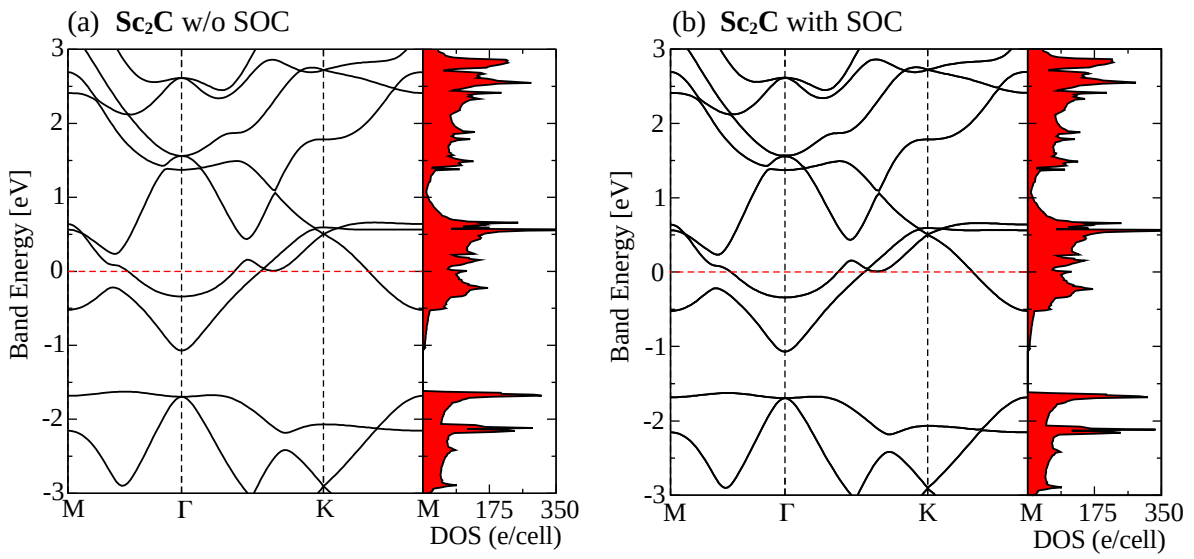


Figure 17: The band structure of Sc_2C with and without spin-orbit coupling, along the high-symmetry directions of the hexagonal Brillouin zone. DOS in electrons/Hartree/cell.

BAND STRUCTURES – NITRIDES

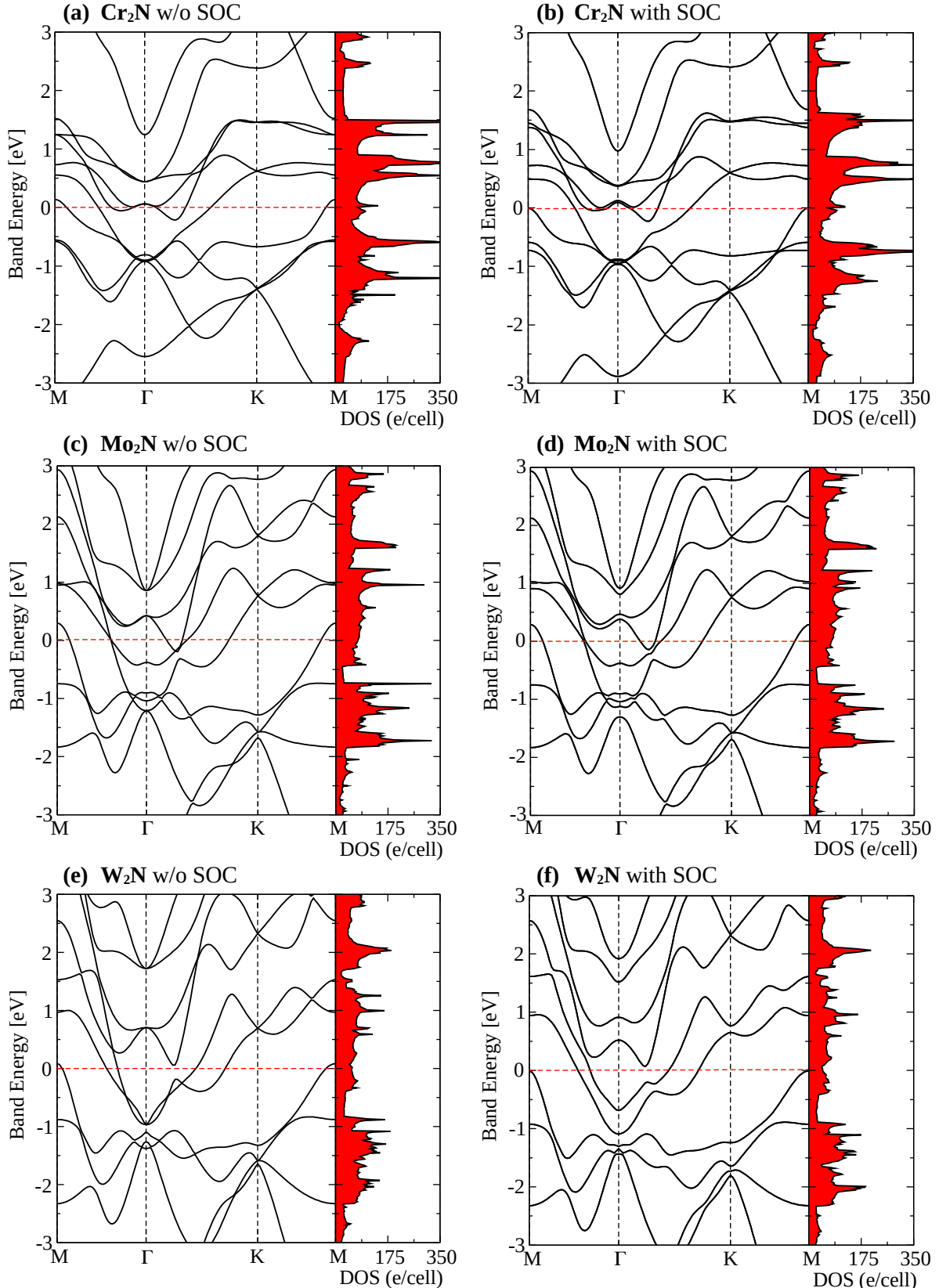


Figure 18: The band structure of M_2N ($M = \text{Cr}, \text{Mo}, \text{W}$) with and without spin-orbit coupling, along the high-symmetry directions of the hexagonal Brillouin zone. DOS in electrons/Hartree/cell.

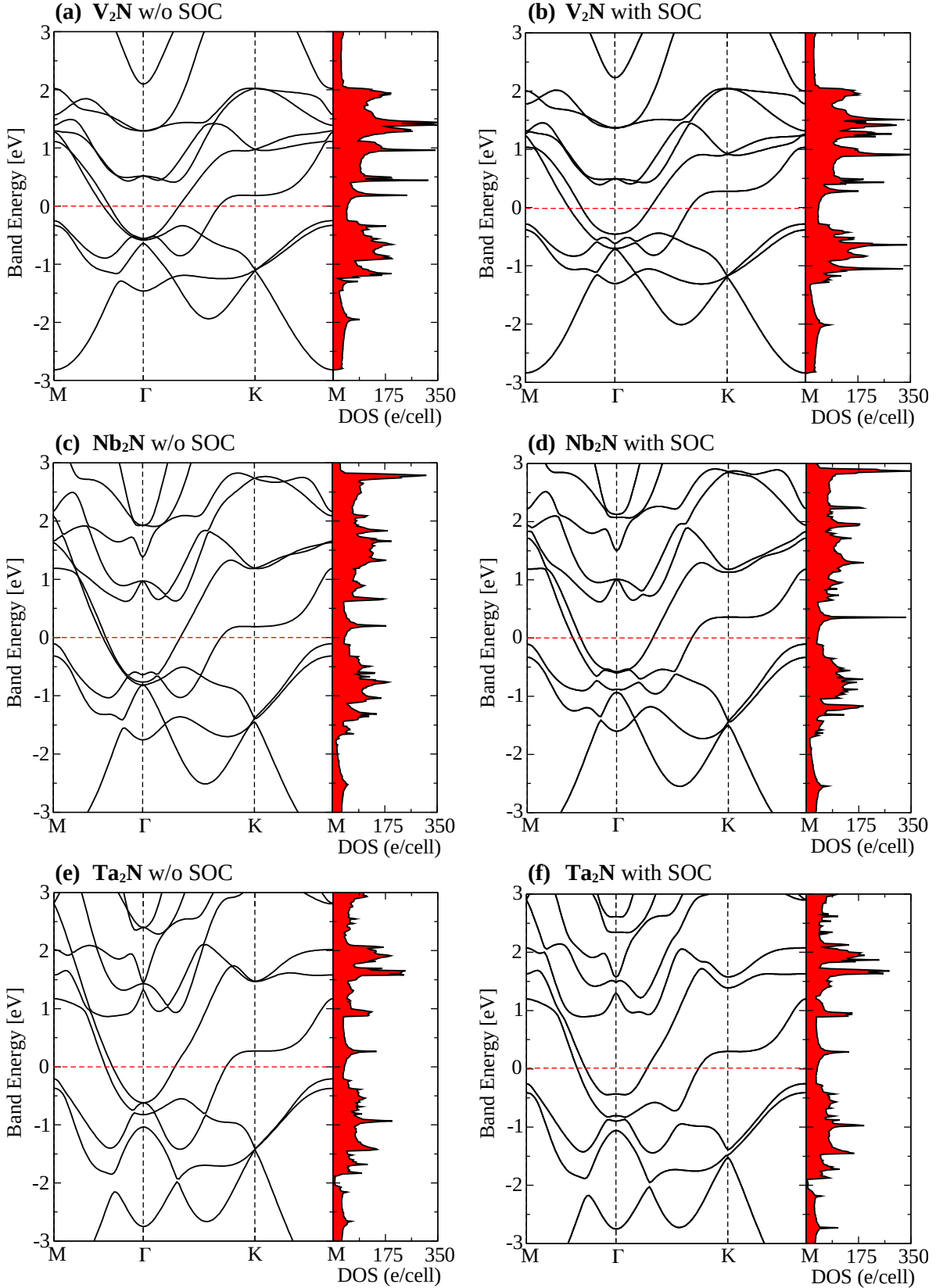


Figure 19: The band structure of M_2N ($\text{M} = \text{V}, \text{Nb}, \text{Ta}$) with and without spin-orbit coupling, along the high-symmetry directions of the hexagonal Brillouin zone. DOS in electrons/Hartree/cell.

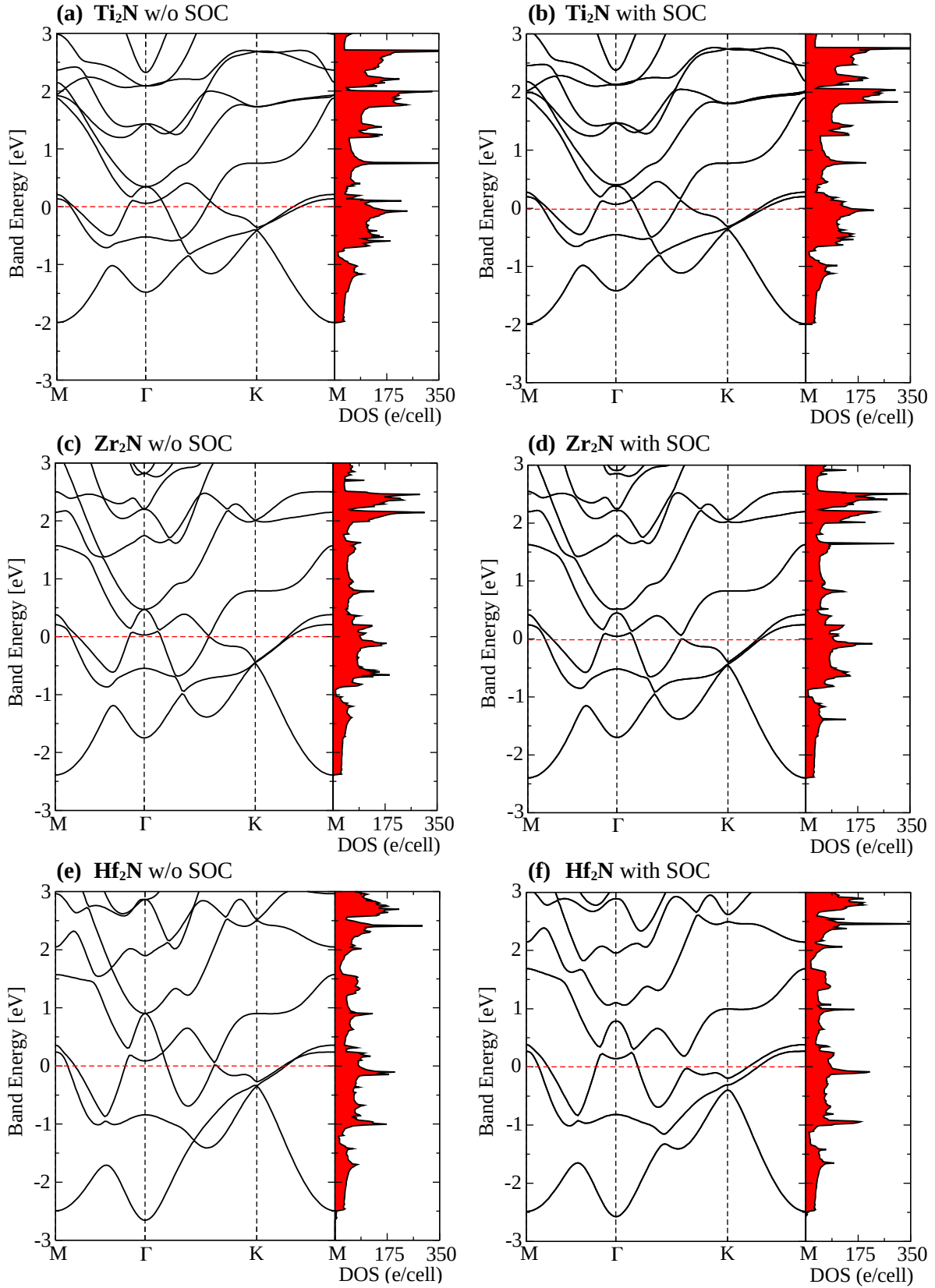


Figure 20: The band structure of $M_2\text{N}$ ($M = \text{Ti}, \text{Zr}, \text{Hf}$) with and without spin-orbit coupling, along the high-symmetry directions of the hexagonal Brillouin zone. DOS in electrons/Hartree/cell.

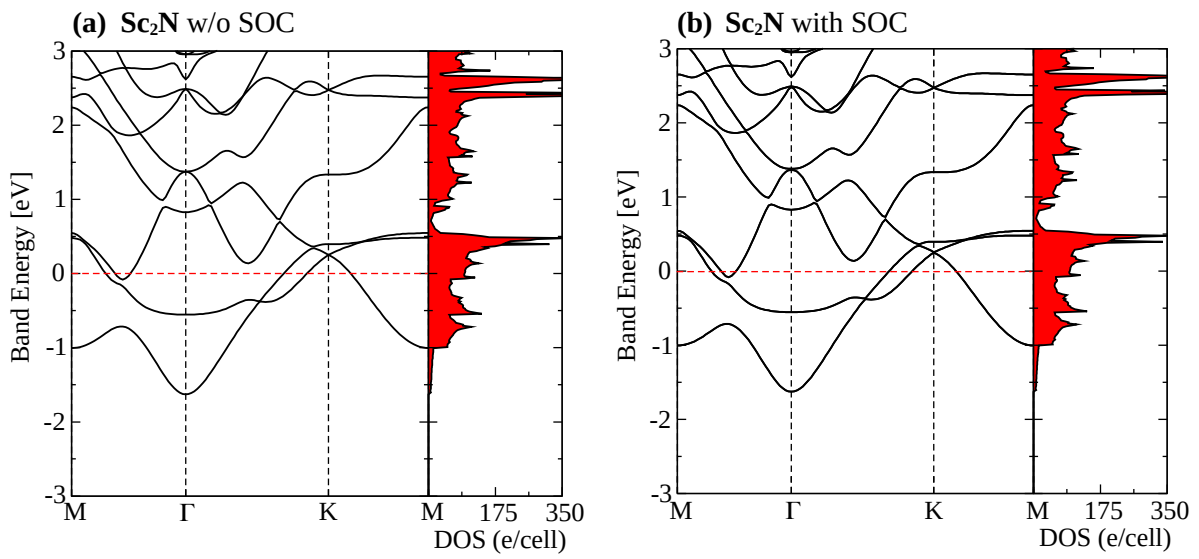


Figure 21: The band structure of Sc_2N with and without spin-orbit coupling, along the high-symmetry directions of the hexagonal Brillouin zone. DOS in electrons/Hartree/cell.

PHONON SPECTRUM – CARBIDES

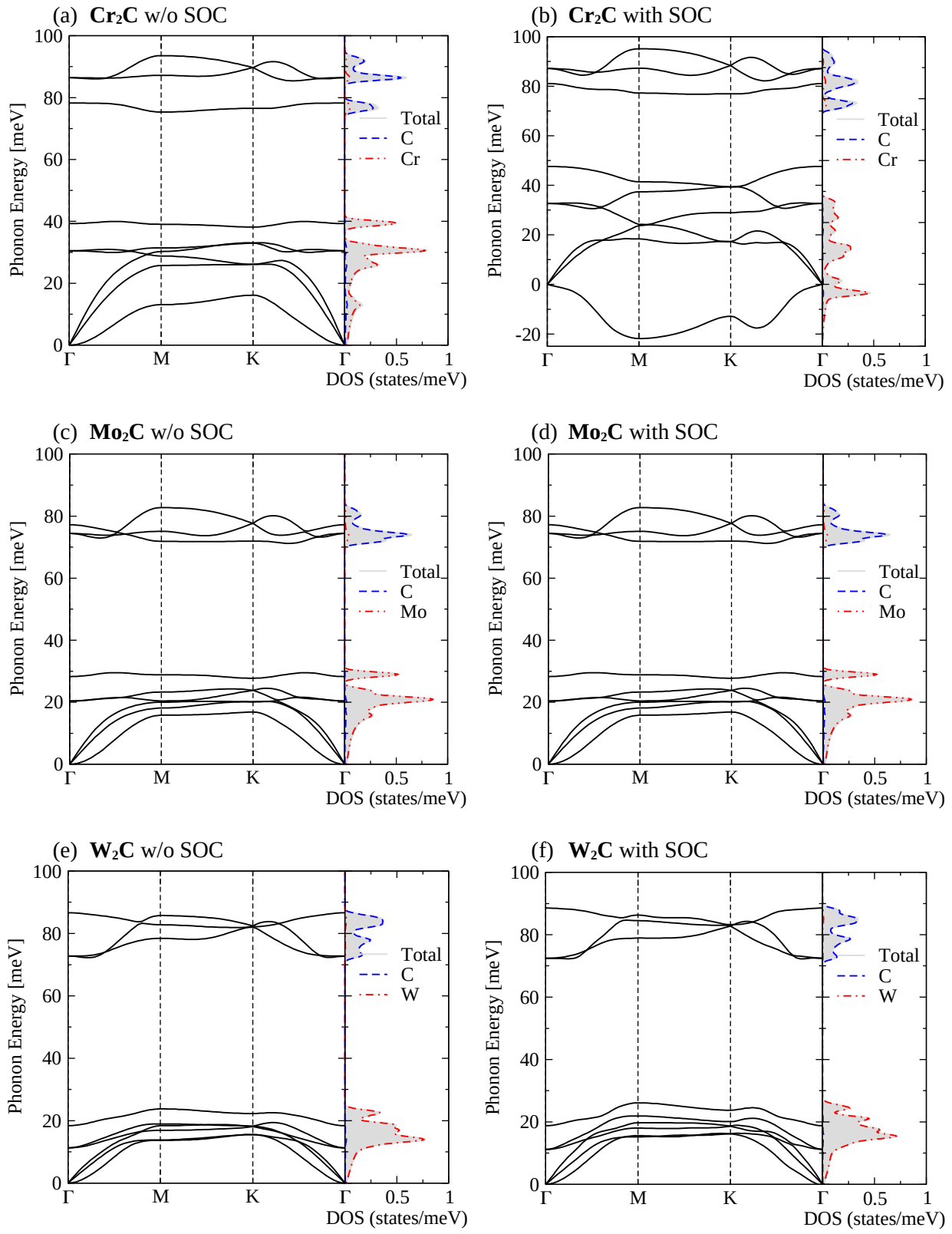


Figure 22: Vibrational spectrum of M_2C ($\text{M} = \text{Cr}, \text{Mo}, \text{W}$) with and without spin-orbit coupling, along the high-symmetry directions of the hexagonal Brillouin zone. DOS in states/meV.

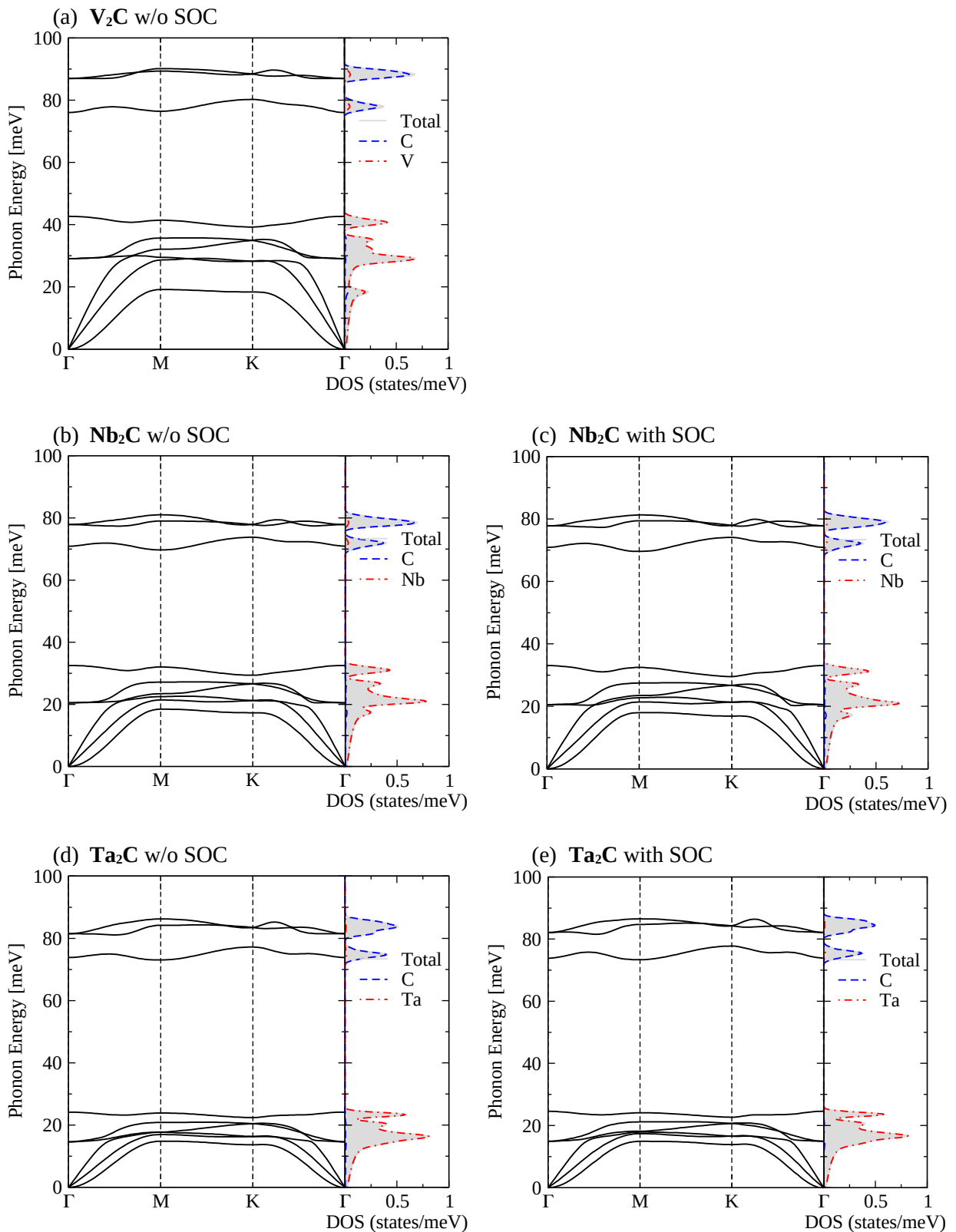


Figure 23: Vibrational spectrum of M_2C ($M = V, Nb, Ta$) with and without spin-orbit coupling, along the high-symmetry directions of the hexagonal Brillouin zone. DOS in states/meV.

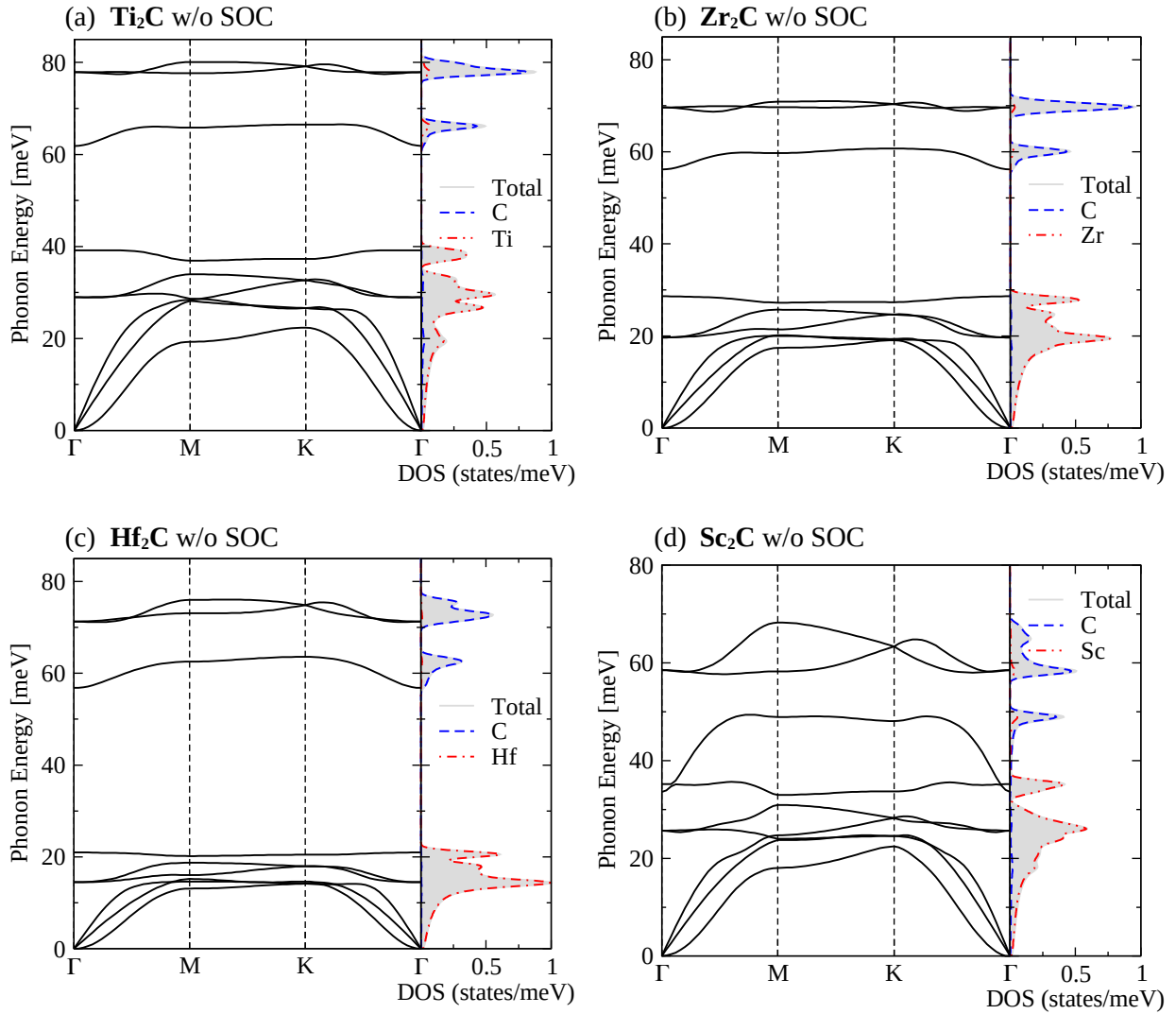


Figure 24: Vibrational spectrum of M_2C ($\text{M} = \text{Ti}, \text{Zr}, \text{Hf}, \text{Sc}$) with and without spin-orbit coupling, along the high-symmetry directions of the hexagonal Brillouin zone. DOS in states/meV.

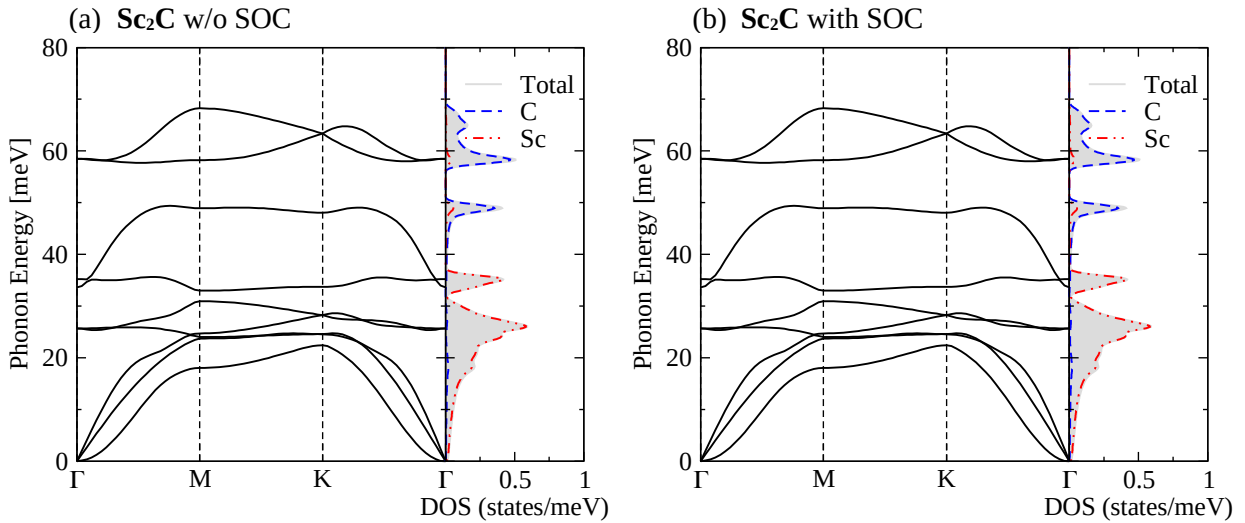


Figure 25: Vibrational spectrum of M_2C ($\text{M} = \text{Ti}, \text{Zr}, \text{Hf}, \text{Sc}$) with and without spin-orbit coupling, along the high-symmetry directions of the hexagonal Brillouin zone. DOS in states/meV.

PHONON SPECTRUM – NITRIDES

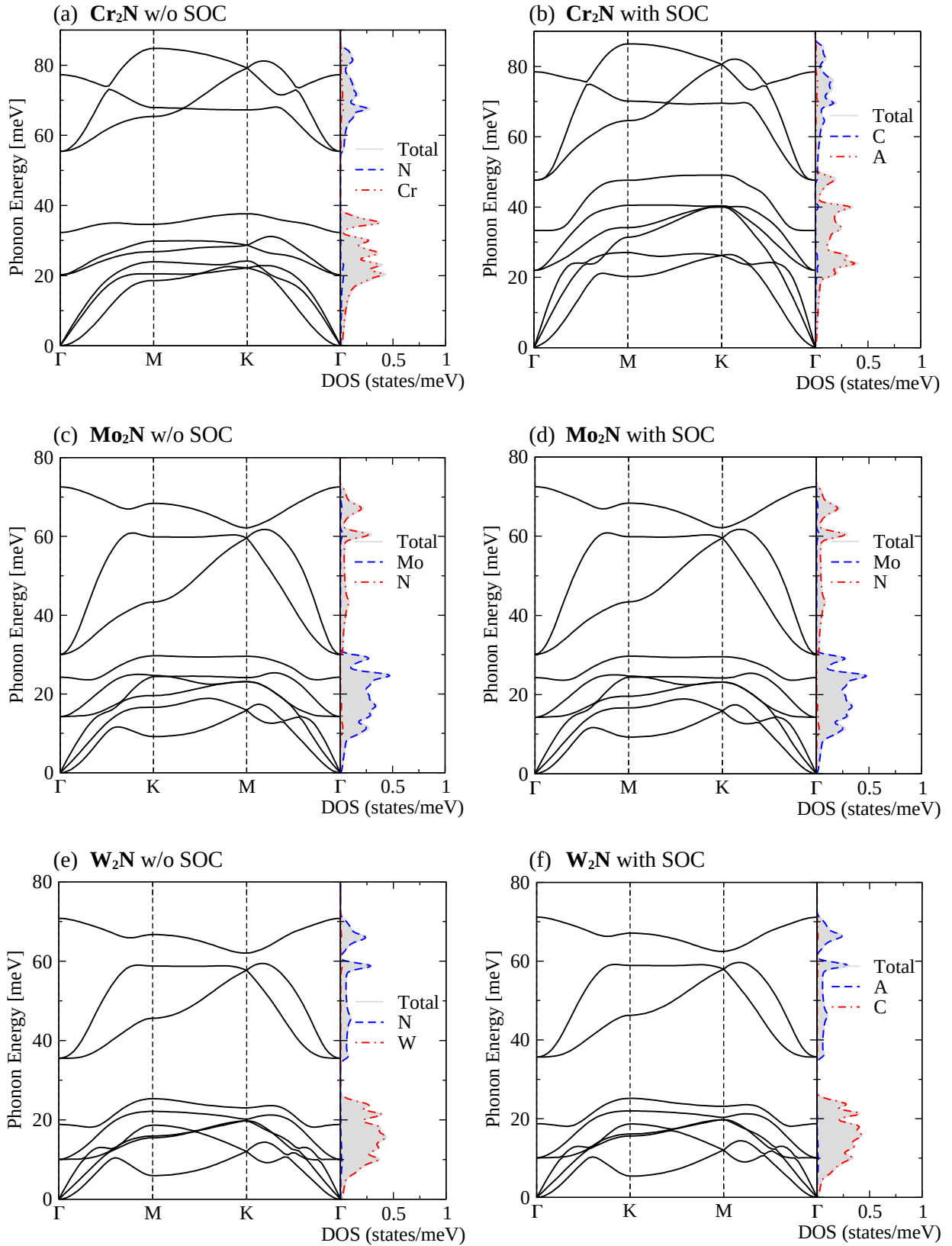


Figure 26: Vibrational spectrum of M_2N ($M = Cr, Mo, W$) with and without spin-orbit coupling, along the high-symmetry directions of the hexagonal Brillouin zone. DOS in states/meV.

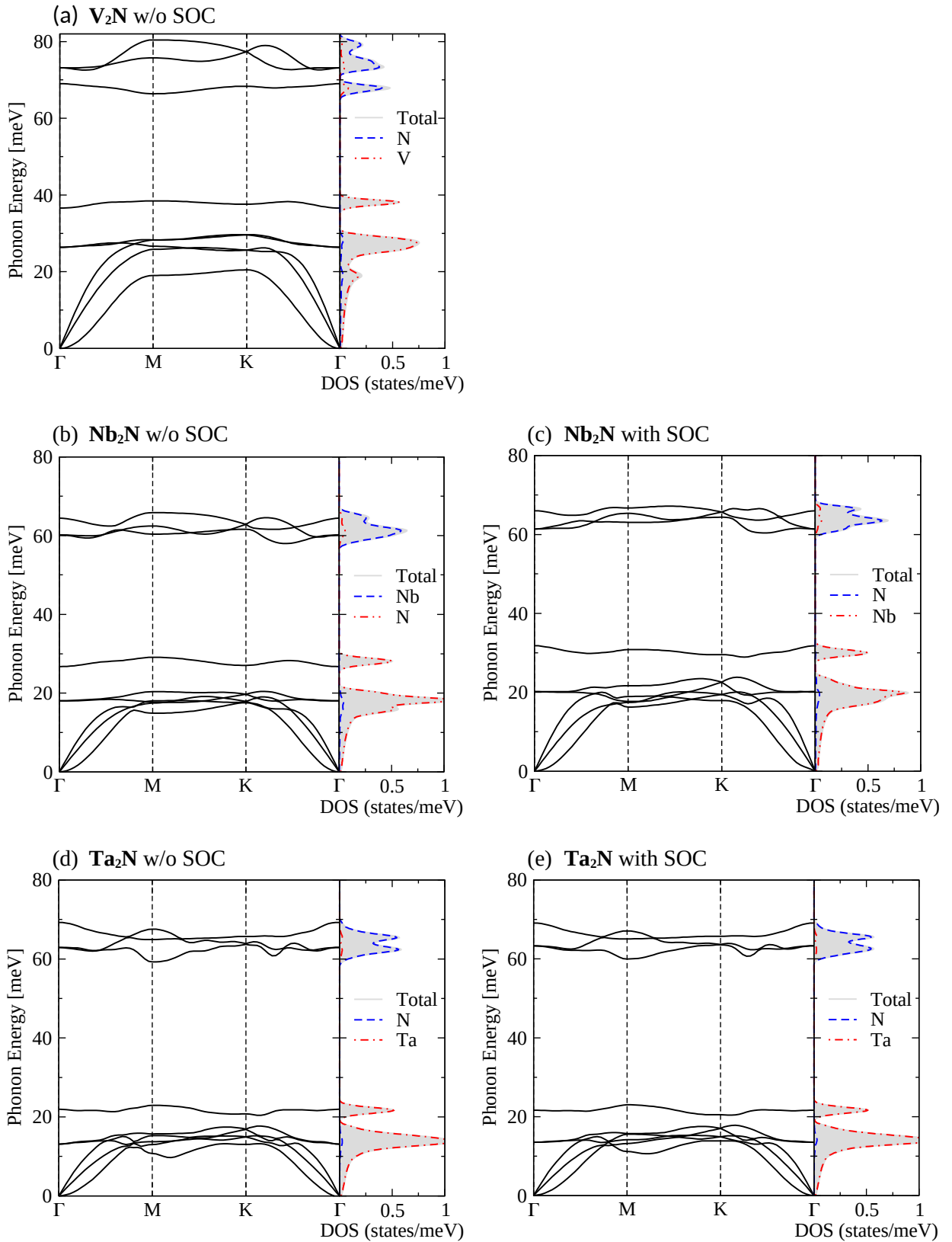


Figure 27: Vibrational spectrum of M_2N ($\text{M} = \text{Cr}, \text{Mo}, \text{W}$) with and without spin-orbit coupling, along the high-symmetry directions of the hexagonal Brillouin zone. DOS in states/meV.

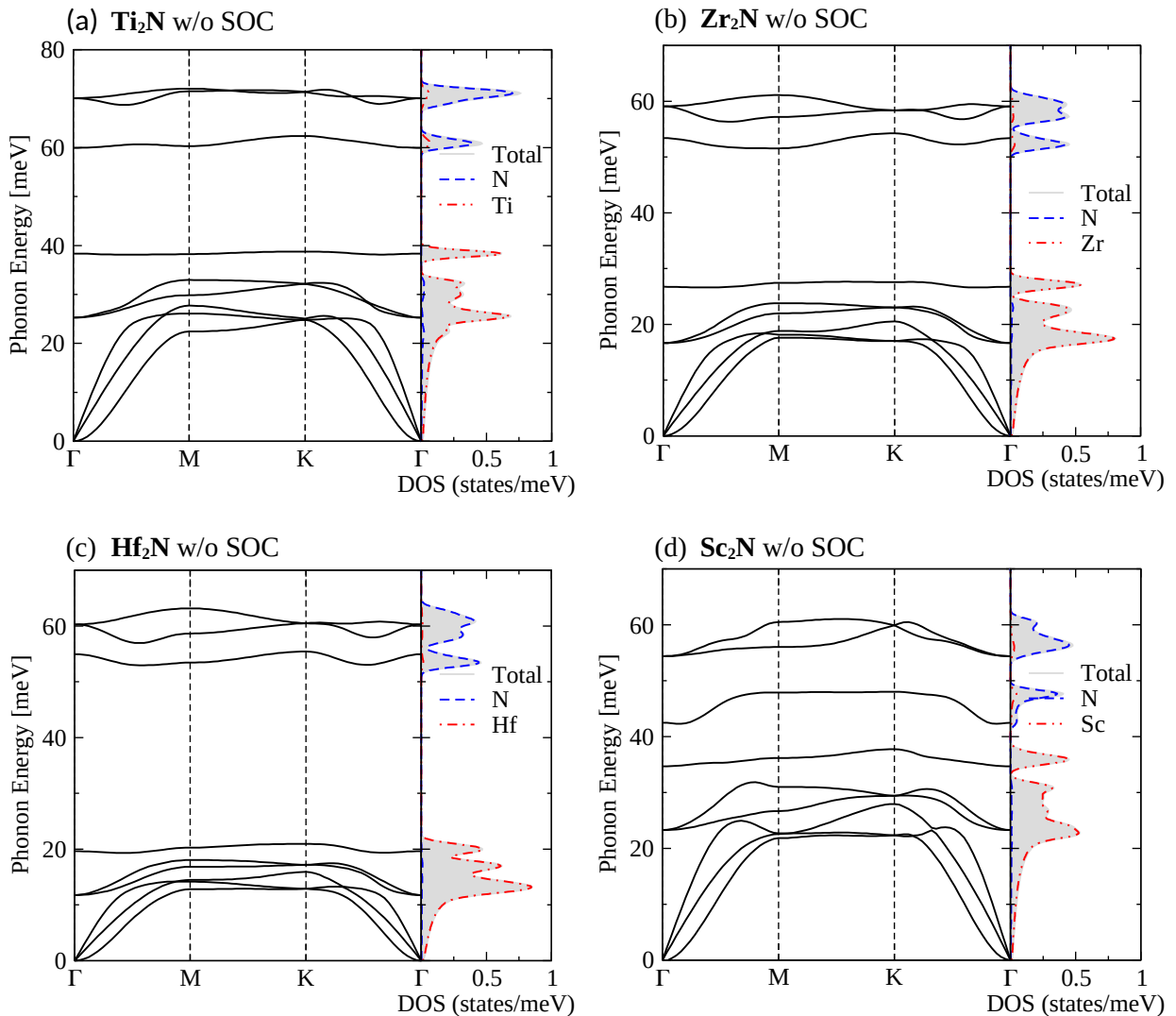


Figure 28: Vibrational spectrum of M_2N ($M = Ti, Zr, Hf, Sc$) with and without spin-orbit coupling, along the high-symmetry directions of the hexagonal Brillouin zone. DOS in states/meV.